ATP Synthase

Wolfgang Junge[1] and Nathan Nelson[2]

[1]Department of Biophysics, Universität Osnabrück, DE-49069 Osnabrück, Germany; email: junge@uos.de

[2]Department of Biochemistry, The George S. Wise Faculty of Life Sciences, Tel Aviv University, Tel Aviv 69978, Israel

Annu. Rev. Biochem. 2015. 84:631–57

First published online as a Review in Advance on March 23, 2015

The *Annual Review of Biochemistry* is online at biochem.annualreviews.org

This article's doi: 10.1146/annurev-biochem-060614-034124

Keywords

F_OF_1 ATPase, photosynthesis, proton transfer, ATP synthesis, chloroplasts, cyanobacteria

Abstract

Oxygenic photosynthesis is the principal converter of sunlight into chemical energy. Cyanobacteria and plants provide aerobic life with oxygen, food, fuel, fibers, and platform chemicals. Four multisubunit membrane proteins are involved: photosystem I (PSI), photosystem II (PSII), cytochrome b_6f (cyt b_6f), and ATP synthase (F_OF_1). ATP synthase is likewise a key enzyme of cell respiration. Over three billion years, the basic machinery of oxygenic photosynthesis and respiration has been perfected to minimize wasteful reactions. The proton-driven ATP synthase is embedded in a proton tight-coupling membrane. It is composed of two rotary motors/generators, F_O and F_1, which do not slip against each other. The proton-driven F_O and the ATP-synthesizing F_1 are coupled via elastic torque transmission. Elastic transmission decouples the two motors in kinetic detail but keeps them perfectly coupled in thermodynamic equilibrium and (time-averaged) under steady turnover. Elastic transmission enables operation with different gear ratios in different organisms.

Contents

INTRODUCTION

Solar Energy Capture by Oxygenic Photosynthesis

Oxygenic photosynthesis is the major energy source of life on Earth. Sunlight is converted into chemical energy and products that humans use as food, fiber, fuel, and platform chemicals. The primary processes of photosynthesis convert sunlight into two forms of chemical energy, namely the redox couple $NADPH/O_2$ and the couple $ATP/ADP + P_i$ (inorganic phosphate). With a stoichiometric ratio of six to nine, these couples drive carbon fixation. NADPH and ATP are used in a six-to-nine ratio for carbon fixation. At the level of these primary products, and in the time domain of microseconds, the efficiency of solar energy conversion can reach up to 20%. Its efficiency is comparable to that of photovoltaic cells (1). In subsequent processes, the efficiency drops to 10% for carbon fixation and to 2% for crops in the field.

In this article and its companion review (2), we describe the structure and function of three major protein complexes, namely photosystem I (PSI), photosystem II (PSII), and ATP synthase (F-ATPase or F_OF_1). They are embedded in the same coupling membrane, composed from several subunits, and have high molecular mass (~600,000 au). Their mechanisms of action are fundamentally different. Photosystems are quantum-mechanical solid-state devices, and F_OF_1 is a mechanochemical machine. In the former, electromagnetic excitation and electrons migrate

between fixed cofactors. The turnover rates are governed by the laws of quantum mechanics. In F_OF_1, intersubunit mobility is the prerequisite for its function as a proton-driven ATP synthase. The dynamics is governed by statistical mechanics, that is, the interplay of stochastic and directed forces.

PSI and PSII are present only in organisms that perform oxygenic photosynthesis (cyanobacteria, algae, and plants), whereas F_OF_1 is present in photoautotrophic and heterotrophic organisms (respiring and nonrespiring bacteria, plants, and animals). F_OF_1 shares its structure and operating principle with a large family of close relatives in chloroplasts, mitochondria, a wide range of bacteria, and yeast. The respective F_OF_1 varieties have different benefits for kinetic and structural examination. For this reason, this article merges data obtained on F_OF_1 from many different organisms.

ATP Production by Photosynthesis and Respiration

In 1958, Racker and colleagues (3) discovered in submitochondrial particles a soluble protein fraction required for coupling the phosphorylation of ADP to the oxidative electron transport chain. They coined it F_1. F_OF_1, or ATP synthase, refers to the combination of F_1 and its membrane-associated counterpart, named F_O (the subscript stands for oligomycin sensitivity). In 1961, Mitchell (4) hypothesized that electron transport crosses the membrane and, being linked to proton transport, generates proton-motive force (PMF) that powers ATP synthesis. PMF is composed of the difference in pH (ΔpH) (4) and in electric potential ($\Delta\varphi$) (5) across the respective coupling membrane:

$$\mathrm{PMF} = \mathrm{F} \cdot \Delta\varphi - 2.3 \cdot \mathrm{R}T \cdot \Delta\mathrm{pH} \quad \text{in units of J/mol}, \tag{1a.}$$

$$\mathrm{PMF} = \Delta\varphi - 60 \cdot \Delta\mathrm{pH} \quad \text{in units of mV}, \tag{1b.}$$

$$\mathrm{PMF} = \frac{\Delta\varphi}{60\mathrm{mV}} - \Delta\mathrm{pH} \quad \text{in units of pH}. \tag{1c.}$$

Here, F denotes the Faraday constant, R the gas constant, and T the temperature in Kelvin. For the in vivo distribution of the PMF over its two components, ΔpH and $\Delta\varphi$, see References 6 and 7.

In thermodynamic equilibrium, the PMF is supposed to match the molar free energy of ATP synthesis, ΔG_{ATP}:

$$n \cdot \mathrm{PMF} = \Delta G_{\mathrm{ATP}} = \Delta G^0_{\mathrm{ATP}} + \mathrm{R}T \ \ln\left(\frac{[\mathrm{ATP}]}{[\mathrm{ATP}] \cdot [\mathrm{P_i}] \cdot [\mathrm{H^+}]}\right). \tag{2.}$$

Here, n denotes the stoichiometric ratio of protons to ATP, $[X]$ is the concentration over the respective (biochemical) standard, and $\Delta G^0_{\mathrm{ATP}} \cong +30.5$ kJ/mol is the standard free energy of ATP synthesis.

In the case of photophosphorylation, experimental evidence in favor of this hypothesis emerged soon after Mitchell's paper (4) was published. Subjecting chloroplasts to an acid–base jump produced ATP (8). The photogeneration of transmembrane voltage was demonstrated by observations of electrochromic effects of intrinsic pigments, which served as a molecular voltmeter (9). The decay of the voltage was quantitatively correlated with ATP production (10). Although Mitchell's hypothesis had been established for photophosphorylation, its validity for mitochondria was heavily debated for quite a while until becoming generally accepted (11).

Boyer and colleagues found that F_1 hosts two or three catalytic sites (12) and might use stored conformational energy for ATP synthesis (13). Rotary action involving three reaction sites was considered as a possibility (14, 15). Several studies reported negative cooperativity for ATP binding with dissociation constants of 1 pM, 30 μM, and 150 μM in beef heart mitochondria (16) and <50 nM, 500 nM, and 25 μM in *Escherichia coli* (17).

F_1 contains five types of subunits in stoichiometric proportion $\alpha_3\beta_3\gamma\delta\varepsilon$ (18). For a long time, investigators did not know how to relate these properties to the enzyme structure nor, in particular, how protons interact with the protein to yield ATP (for this history, see Reference 19 and references therein). The function of F_1 could not be understood without knowledge of its crystal structure (see the section titled Structure of F_1, below). We now know that F_OF_1 is composed of two rotary nanomotors: the ion-driven, electrochemical F_O and the chemical F_1, which are mechanically coupled (reviewed in References 20–25).

Architecture of the Coupling Membrane

The coupling membranes of oxygenic photosynthesis contain PSI, PSII, the cytochrome b_6f complex (cyt b_6f), and F_OF_1 (**Figure 1*a***). The primary photochemical electron transfer in both PSII and PSI, and the secondary transfer in cyt b_6f, is directed from the positively charged side

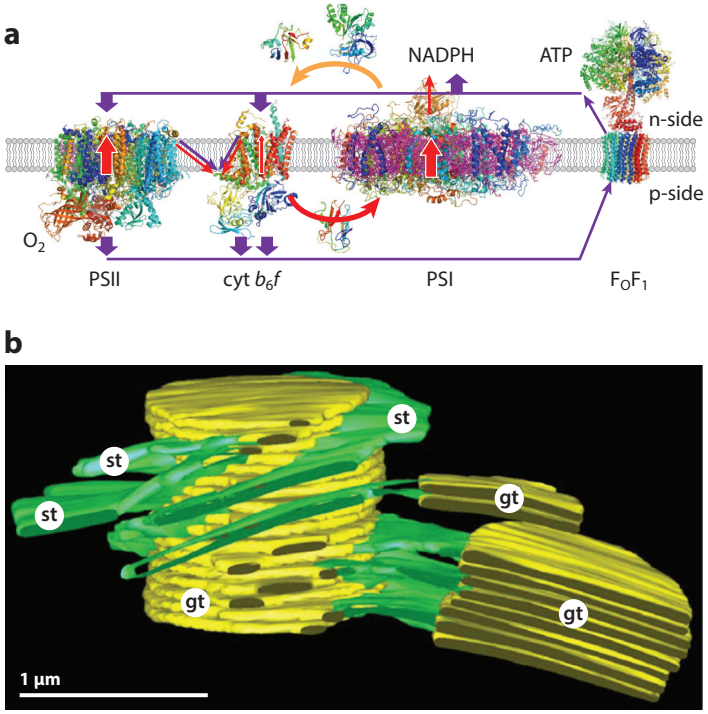

Figure 1

Electron and proton transfer in the thylakoid membrane. (*a*) Electron transfer (*red arrows*) and proton transfer (*purple arrows*) involving photosystems I and II (PSI and PSII), cytochrome b_6f (cyt b_6f), and ATP synthase (F_OF_1), and producing O_2, NADPH, and ATP. (*b*) The folding of thylakoid membranes in chloroplasts, based on electron tomography. Abbreviations: gt, grana thylakoid membrane; st, stroma thylakoid membrane. Modified with permission from from Reference 33.

(p-side) to the negatively charged side (n-side) of the membrane (9, 26, 27). Proton uptake (n-side), oppositely directed hydrogen transfer, and proton release (p-side) acidify the p-side over the n-side and contribute further to the PMF, which drives ATP synthesis by F_OF_1.

The photosynthetic coupling membrane is highly crowded. With a specific membrane area of ~2 nm^2 per chlorophyll molecule (28) and ~1,000 chlorophyll molecules per PSI:PSII:cyt b_6f:F_OF_1 in the approximate proportion 2:2:1:1, the mean area per large complex amounts to less than 200 nm^2. In chloroplasts of green plants, the coupling membrane is folded into flattened sacs, named thylakoids (29), that are piled up into grana and linked together by intergrana (or stroma) lamellae (**Figure 1*b***). The whole membrane system inside a chloroplast can be unfolded into one large spherical bleb (28). Also, a single dimer of the powerful ionophore gramicidin per more than 10^7 chlorophyll molecules accelerates the decay of the transmembrane voltage (30). In other words, this intricately folded system seems to form a single, simply connected sheet (in mathematical terms) such that more than 10^4 electron transport chains and ATP synthase molecules are electrically coupled with one another. For decades, investigators have argued that stroma lamellae helically outgrow from grana stacks (31). Ongoing research by high-resolution electron tomography (32–34) supports this idea (**Figure 1*b***). How such a structure can unfold into a large spherical bleb (either intrinsically or via fractionation and fusion) is still unknown. Biochemical analyses (35), freeze-fracture electron microscopy (36), and more recently electron tomography (with up-to-5-nm resolution) (33, 37) established the nonhomogeneous lateral distribution of the membrane proteins. PSI and F-ATPase are located mainly in the stroma lamellae, as well as in the top and bottom surfaces of grana. PSII is found almost exclusively inside grana, and the cyt b_6f complex is found in grana and at grana margins (35, 37, 38). The lateral separation of PSII and PSI is beneficial for three reasons: It prevents their competition for light (39), facilitates regulation of the distribution of light (40), and facilitates repair of PSII after photodamage (2). How the lateral separation between the producers (PSII, PSI, cyt b_6f) and the consumer (F_OF_1) of PMF bears on the efficiency of ATP synthesis is discussed in the section titled The Enzyme in the Coupling Membrane, below.

F_1, THE CHEMICAL MOTOR

Structure of F_1

Walker and colleagues (41) used bovine mitochondria to obtain the first asymmetric crystal structure of F_1. The original resolution of 2.8 Å was later advanced to 1.9 Å (42). The crystal structure unveiled the determinants of rotary catalysis by F_1 (**Figure 2*b***). The α- and β-subunits are arranged in alternation into a pseudohexagon, $(\alpha\beta)_3$; the γ-subunit is a shaft in its center. One nucleotide is bound to each of the three α-subunits without any known role in catalysis and regulation. The three β-subunits differ in that one is empty (β_E); one is loaded with MgADP (β_{DP}); and the third, named β_{TP}, is loaded with a nonhydrolyzable ATP analog. The central shaft of the γ-subunit is cranked. Its convex side pushes the helix-turn-helix motif at the C-terminal end of the β-subunit (hereafter referred to as the hinge) to expose and empty the respective nucleotide-binding site. This structural model may explain how the three (in principle) equivalent reaction sites cooperate in hydrolyzing ATP to yield ADP and P_i. The three sites perform different steps in the sequence involving the binding of ATP, ATP hydrolysis, and product release, and their roles change cyclically. The empty site, β_E, supposedly binds a new molecule of ATP; the cranked shaft is driven forward toward β_{DP}; and the convex side of the γ-subunit pushes the hinge on β_{DP} to extrude the products of hydrolysis, ADP and P_i. ATP, which is bound to the β_{TP} site, is split into bound ADP and P_i.

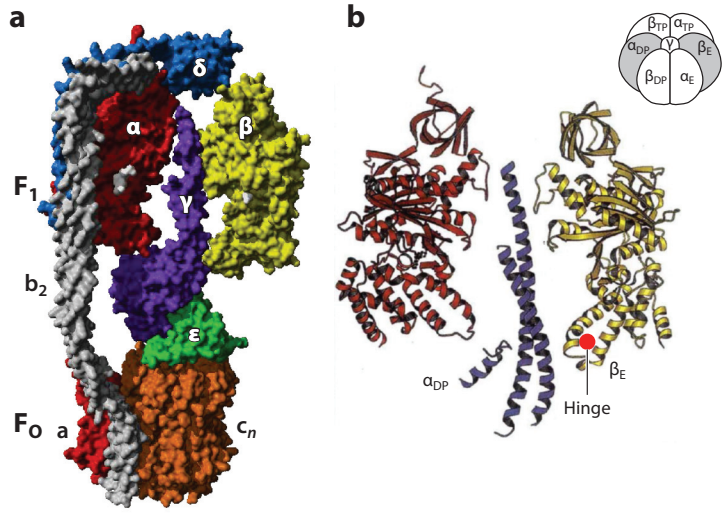

Figure 2

Structural models of the ATP synthase. (*a*) Homology model of F_OF_1 from *Escherichia coli*. The F_1 and F_O portions and the subunit composition, $(\alpha\beta)_3\gamma\varepsilon\delta c_{10}ab_2$, are indicated. For $(\alpha\beta)_3$ (*orange*), only one copy of the β-subunit, β_E, and one copy of the α-subunit are shown. (*b*) The first asymmetric crystal structure of $(\alpha\beta)_3\gamma$ from bovine mitochondria (41). The red dot marks the helix-turn-helix motif of the β-subunit, the hinge.

The Walker group has analyzed many other crystals grown in media with or without specific inhibitors and various nucleotide analogs (reviewed in Reference 24). Most of these crystals resemble the ground-state structure (42), in which one site, β_E, is empty and the other two sites, β_{DP} and β_{TP}, are filled with nucleotides. The nucleotide-binding pockets of the β-subunit is lined by the so-called Walker motif, GxxxxGKT/S (where x refers to any residue) (43), which was later also found in other nucleotide-binding proteins. Another characteristic of the binding pocket is an arginine finger, which is contributed by the adjacent α-subunit (41). The arginine finger coordinates the γ-phosphate in β_{TP} and turns away from this position in the absence of ATP. A related situation exists in Ras GTPase, in which phosphoryl transfer is electrostatically facilitated by an arginine finger, again provided by a companion protein (44).

Among several crystal structures of bovine F_1, only two differ from this pattern. In these cases, all three sites contain nucleotides (45, 46). Both structures have been interpreted as intermediate states of ATP hydrolysis. In the first structure, the sites equivalent to β_{DP} and β_{TP} carry MgADP · AlF_4^-, supposedly a transition-state analog, and the third site, β_E, carries MgADP. An immobilized water molecule, supposedly used for nucleophilic attack, appears on the γ-phosphate of ATP (45). In the second structure the β_{DP}- and β_{TP}-equivalent sites contain nucleotides, and a half-closed β_E site contains only ADP (no magnesium or phosphate). It has been interpreted as a posthydrolysis, pre-nucleotide-release state (46). Evidence suggests that, of the two products of ATP hydrolysis, phosphate leaves first and ADP second (for a contrasting opinion, see the section titled Stepped Rotation Related to Crystal Structure, below).

The general discussion of the kinetics and mechanism of F_1 from all organisms is based largely on structures of the bovine enzyme. The few structural models of $(\alpha\beta)_3\gamma$ that come from other sources are basically similar to the bovine model but differ in detail. All three structures refer to nucleotide-free F_1. In chloroplast F_1 [at 3.2-Å resolution (47)], all three β-subunits are in a

closed conformation; in thermophilic *Bacillus* F_1 [at 3.1-Å resolution (48)], they are in an open conformation; and in yeast F_1 [at 3.6-Å resolution (49)], one nucleotide site is open and two are closed. The reason for the conformational differences between these nucleotide-free enzymes is not yet understood. The only structure of *E. coli* F_1 to date represents an ε-inhibited state of the $(\alpha\beta)_3\gamma\varepsilon$ entity [at 3.26-Å resolution (50)]. In this structure, only one nucleotide of F_1 is bound—the two other sites are filled with SO_4^{2-}—and the hinge points to an α-subunit rather than to a β-subunit. For the regulation of F_OF_1 by the ε-subunit in bacteria, see the section titled Regulation, below.

ATP Hydrolysis Drives the Rotation of the Central Shaft

The first crystal structure described above prompted investigators to pursue real-time recording of rotary motion. Cross and colleagues (51) used a biochemical assay to show that the γ-subunit changes its position relative to the three β-subunits when hydrolyzing ATP, however, without time resolution. By using polarized photobleaching and recovery, Junge and colleagues (52, 53) demonstrated the rotation of the γ-subunit relative to $(\alpha\beta)_3$ in real time. Yoshida, Kinosita, and their colleagues (54) made a video recording of the rotation of the γ-subunit in single molecules of F_1. These authors fixed F_1 from *Bacillus* PS3 head down on a solid support and attached a fluorescent actin filament to the "foot" of the γ-subunit. They monitored the rotation of the probe with fluorescence microscopy. Their video-microscopic technique became the gold standard in the field. It demonstrated that hydrolysis of ATP turns the central shaft counterclockwise when viewed from the membrane. With a short probe (F-actin or bead) on the enzyme, the rate of rotation is not severely limited by viscous drag. Steps and dwells on the reaction path became apparent (55). The observed period of 120° reflects the threefold pseudosymmetry of $(\alpha\beta)_3$ and is subdivided by steps of 90° and 30° starting from the ATP-waiting dwell and the catalytic dwell, respectively. The catalytic dwell before the 30° step is composed of two mechanically silent subreactions, each ~1 ms long (55). The width of the substeps was later modified to 80° and 40° (56, 57). The nucleotide occupancy, conformational changes of the β-subunit, and rotation of the central shaft were monitored in parallel (58, 59). The 80° rotation is concomitant with (driven by) ATP binding and ADP release, and the 40° step is concomitant with (driven by) phosphate release and the hydrolysis of bound ATP. A freshly bound ATP molecule leaves the enzyme as ADP only after the central shaft has turned forward by 240° (58, 60–62). This stepwise motion has also been demonstrated in *E. coli* F_1 (63–66). In human F_1, an additional dwell and slightly different dwell angles have been reported (67).

The time resolution of stepped rotation has been greatly improved by use of a gold nanorod (typically 30 nm long) as a probe on the rotor. The rotation was detected at microsecond resolution via the polarization of scattered light (68–70).

Stepped Rotation Related to Crystal Structure

Stepped rotation of the γ-subunit in single-molecule experiments cannot be related a priori to the orientation of $(\alpha\beta)_3$ in lab coordinates and, thereby, to the crystal structure. Three research groups have overcome this drawback. Two of them (66, 71) recorded rotary stepping and then locked the rotor to the stator (by a disulfide bridge) in a position similar to the one in the crystallographic position aiming at the ground state of the bovine enzyme (**Figure 3*a*,*b***). The third group used fluorescence resonance energy transfer (FRET) (59). All three groups found that the rotor orientation in the crystal structure of the bovine enzyme corresponds to the catalytic dwell in the

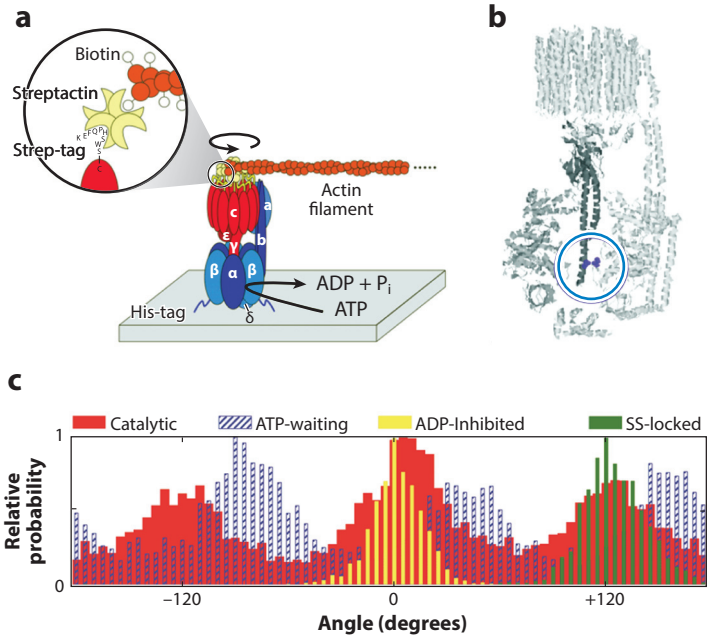

Figure 3

Stepping of F_OF_1 when driven by ATP hydrolysis. (*a*) Isolated and immobilized F_OF_1 with fluorescent actin filament attached to the c-ring of F_O (135). (*b*) Engineered disulfide bridge (*inside the blue circle*) intended to trap the rotor orientation, as in crystals (see **Figure 2*b***). (*c*) Histogram over 360° of the rotary stepping under ATP-limited conditions (*hatched blue*) and when dominated by catalysis (*red*). The position of the rotor in the inactive enzyme is blocked either by ADP (*yellow*) or by the disulfide bridge (*green*) (66). The term SS-locked denotes the closed disulfide bridge.

respective bacterial enzyme rather than to the ATP-waiting dwell. In *E. coli* F_1, this orientation coincides with that of the ADP-inhibited state (66). In the ATP-waiting dwell, the rotor is turned forward (counterclockwise) by more than 40° (**Figure 3*c***).

The forward displacement of the ATP-waiting dwell was an unexpected result that prompted checks for possible packing deformations in crystals. The "foot" of the γ-subunit is susceptible for contortion by up to 35° (46), but the remainder is not (24). The distortion of the foot has led to the belief that the crystallographic results are difficult to reconcile to the discrete states observed in single-molecule biophysical experiments (24). This belief does not hold. Although the foot of the γ-subunit may be contorted in crystals, in active single molecules it thermally relaxes during dwells. [This relaxation has been used to determine the elastic parameters of F_OF_1 (25, 65, 66).] In other words, a small probe that is directly (71) or indirectly (**Figure 3*a***) (66) attached to the foot region can correctly indicate the orientation of the central stalk during dwells. The width of the fluctuations around the mean position monitors the torsion spring constant of the transiently resting enzyme during the dwell (**Figure 3*c***) (66).

Figure 4 illustrates a model for the sequence of events over one full turn of the central stalk and the hydrolysis of three molecules of ATP. Whether phosphate or ADP is first released from the very reaction site where it is produced during the catalytic dwell is a matter of debate. Each view—namely phosphate first and ADP second (**Figure 4*a***) (46, 72) or ADP first and phosphate second (**Figure 4*b***) (61, 73)—is backed up by circumstantial structural and kinetic evidence. Recently, investigators used targeted molecular dynamics (MD) in an attempt to determine what makes

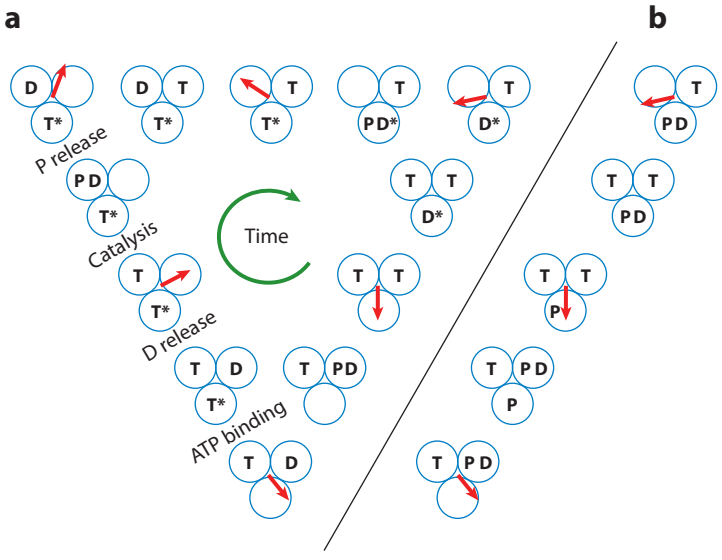

Figure 4

A full reaction cycle of ATP hydrolysis by three cooperative reaction sites in F_1. The three sites cyclically change their role from binding ATP over hydrolysis to liberating the products ADP and inorganic phosphate. The occupation of the three reaction sites by ATP (T), ADP (D), and phosphate (P) is indicated. The reaction proceeds clockwise (*green arrow*). During a full reaction cycle, the central shaft (*red arrow*) turns counterclockwise. The tip of the red arrow denotes the apex position of the convex side of the γ-subunit (see **Figure 1*b***). In the ATP-waiting dwell of the active enzyme, it is displaced by +40° (counterclockwise) forward (59, 66, 71) from the position in the first crystal structure (41). The oblique column in panel *b* parallels its neighbor to the left, except that the sequence of product release after hydrolysis is changed from phosphate first in the triangle to ADP first in the column.

these versions different (74). The authors studied the energy profile of the release of P_i^{2-} from the binding pocket, with an emphasis on its interaction with the arginine finger. The release of P_i^{2-} from β_E is kinetically feasible in the time range of milliseconds, whereas that from β_{DP} is not. P_i^{2-} release from β_E (in ~1 ms) turns the γ-subunit by 40°. This transition might kinetically slave the catalytic step in β_{DP}. In other words, waiting for the release of P_i^{2-} from β_E, and not catalysis proper, might define the duration of the catalytic dwell. The binding of ATP occurs only after the 40° turn, when the β_E site is unoccupied and in a semiopen conformation (**Figure 4*a***).

How many nucleotide molecules occupy the enzyme at its three catalytic sites is under debate. Some researchers claim three (ATP-to-ADP ratio of one to two) on the basis of ensemble experiments in which engineered tryptophan in the binding pocket serves as a probe for occupancy (75, 76). Other authors claim two on the basis of single-molecule experiments with fluorescent ATP analogs (58, 77). The seemingly conflicting views are likely compatible with each other given that the former experiments used physiological (i.e., high) nucleotide concentrations versus low nucleotide concentrations in the latter studies. At physiological concentrations, β_E may bind nucleotides with low affinity.

Investigators have established the reversibility of the chemomechanical coupling in F_1 by magnetically reversing the rotation of the central shaft (with attached paramagnetic bead) and producing detectable amounts of ATP in femtoliter chambers (78, 79). Recently, the magnetic drive was used to first force the shaft into a given position, then release the constraint and monitor

the relaxation of the cooperative reactions in $(\alpha\beta)_3\gamma$ to either side. This is an interesting way to further elucidate the energy landscape as a function of angle (62).

Structural Determinants of Rotary Function

The chiral activity of F_1 may be determined by $(\alpha\beta)_3$, the coiled coil of the γ-subunit, and/or their interaction. The activity of bare $(\alpha\beta)_3$ (without the γ-subunit) was recently studied by time-resolved atomic force microscopy (80). In the presence of MgATP, the three copies of the β-subunit undergo cyclic conformational changes in the same direction as when the γ-subunit was present. Therefore, bare $(\alpha\beta)_3$ is intrinsically chiral and active, although at a much lower rate than in the presence of the γ-subunit. The $(\alpha\beta)_3$ of F_1 is just one example of nature's wide use of hexagonal nucleotide triphosphatases (A-, F-, and V-ATPases; helicases; bacterial DNA translocases), which rotate and/or translocate proteins, RNA, and DNA in their central cavity and probably share common ancestry with F_1 (81).

The role of the coiled coil on the γ-subunit in the direction of the rotation, and the minimum structure of γ-subunit necessary to pick up torque, has been studied through successive truncation. The *E. coli* enzyme tolerates the truncation only of the C-terminal end of the γ-subunit, the shaft in the hydrophobic bearing of $(\alpha\beta)_3$ (82). F_1 from *Bacillus* PS3 is more robust. It tolerates the elimination of 36 residues from the C terminus of the γ-subunit (83) and 50 residues from the N-terminal end (84), and it still produces sizable torque. Accordingly, the coiled coil of the γ-subunit is not essential for chiral operation. What about the remainder of the γ-subunit, which is in close contact with the C-terminal hinge? The partial truncation of the β-subunit's hinge domain (85) and extensive mutations of the contact surfaces between the γ-subunit and the hinge on the β-subunit (86) reduce the magnitude of torque but do not fully eliminate its production.

All-atom 300-ns MD simulations of the nucleotide-free F_1 (87) reveal that a fully open conformation of the hinge, as in β_E (41, 42), is not stable, as had been previously assumed (22, 88). Rather, this conformation is enforced by the interaction between the C-terminal helix-turn-helix motif of the β-subunit and the convex surface of the γ-subunit. The most stable conformation of β_E is half-open. The elastic relaxation of the hinge from the former into the latter conformation has a vector component perpendicular to the axis $(\alpha\beta)_3$ so that it turns the γ-subunit forward by $>40°$ in the hydrolysis direction (87). The relaxed, half-open conformation might represent the ATP-binding dwell, as indicated by kinetic single-molecule experiments on the active enzyme (59, 66, 71).

These observations suggest that the off-axial motion of the C-terminal helix-turn-helix motif of the β-subunit (the hinge) may be the major determinant of the chiral activity of F_1. Its contact with the convex surface of the γ-subunit in F_1—or with some other component in related hexagonal nucleotide triphosphatases—is required to transmit torque and, apparently, to speed up the enzyme activity.

Torque and Efficiency

The magnitude of the torque generated by the hydrolysis of ATP has been determined by single-molecule experiments in two ways. In the first approach, the rate of rotation of probe is recorded, and the torque, τ, is calculated from the angular velocity, ω, and the friction coefficient of the probe, f, by the relation $\tau = f \cdot \omega$. The friction coefficient is usually calculated for the viscosity of the bulk medium (54, 64). Thus, the torque is systematically underestimated. Viscous flow coupling between the rotating probe and the surface is difficult to assess but cannot be neglected. This problem is overcome by the second approach, which uses a long (typically 3-μm) actin filament

attached to the central shaft to slow the rate of rotation by orders of magnitude. Thermodynamic equilibrium between the enzyme and the elastic probe is approximated. The curvature of the filament serves as a spring balance to gauge the torque without a need to know the viscous damping (89, 90). The filament's spring constant is obtained from its thermal fluctuations. The mean torque, when determined by this method, is greater than that determined from the first approach. The magnitude, $\tau = 55$ pN·nm, matches the driving force of ATP hydrolysis. In quantitative terms,

$$3 \cdot \Delta G_{ATP} = 2\pi \cdot \tau \cdot N_A. \quad 3.$$

Here, ΔG_{ATP} denotes the molar free energy of ATP hydrolysis under the given conditions (70 kJ/mol), τ is the torque (55 pN·nm), N_A is the Avogadro number, and the numerals account for the fact that three ATP molecules are hydrolyzed when the γ-subunit rotates by 2π (for the torque profile as a function of angle, see Reference 90 and the section titled Elastic Transmission of Torque, below). The finding that the chemical free energy matches the mechanical energy that is elastically stored in the actin filament implies that the chemical-to-mechanical energy transduction in F_1 has an efficiency of 100%. In other words, the γ-subunit does not slip relative to $(\alpha\beta)_3$. Slip has been observed only at very low nucleotide concentrations, when the $(\alpha\beta)_3$ hexagon apparently loosens its grip on the γ-subunit (91, 92). At physiological nucleotide concentrations, there is no slip in either F_1 or F_OF_1.

Modeling F_1 Dynamics

With a wealth of crystal structures at atomic resolution, detailed kinetic information at submillisecond time resolution, and video recordings of the rotary procession, F_1 can be considered a "hydrogen atom" of biological nanomotoring. Its dynamic behavior depends on the interplay between organizing forces and a disorganizing stochastic force. The former are either conservative (e.g., Coulomb force) or entropic (concentration dependent), and the latter results from thermal impact (Langevin force). Stochastic force affects the turnover rates, whereas the mean directionality of the reactions is fully determined by the organizing forces.

Several groups have attempted to describe F_1 in terms of atomic coordinates by all-atom explicit-solvent MD (see Reference 74 and references therein). These approaches have suffered from the need to apply a higher-than-physiological torque to the central stalk in order to squeeze the events into a narrow time frame (~100 ns). Mukherjee & Warshel (93) overcame this drawback by using a coarse-grained approach. Using advanced electrostatic approximations, they reproduced the counterclockwise rotation with 80° and 40° steps in a reasonable time frame. Karplus and colleagues (see Reference 94 and references therein) merged a coarse-grained approach with biochemical data on nucleotide binding. So far, most theoretical attempts on F_1 have described what has already been observed; however, they can be predictive (for a predictive mutation in silico, see Reference 87).

F_O, THE ELECTROCHEMICAL MOTOR

Structure of F_O

In *E. coli*, F_O is composed of three different subunits in the stoichiometric proportion $c_{10}ab_2$. A high-resolution structure of the entire F_O is lacking. Common to the F_O portion of the ATP synthase of all organisms is a homo-oligomeric ring of the c-subunit, the only portion of F_O for which high-resolution structures are available (see **Figure 5*a*,*b*** and Reference 95 for the Na^+-binding ring of *Propionigenium modestum*, Reference 96 for yeast, and Reference 97 for chloroplasts). So far, the best resolution of the mutual arrangement of the c-ring and the a- and

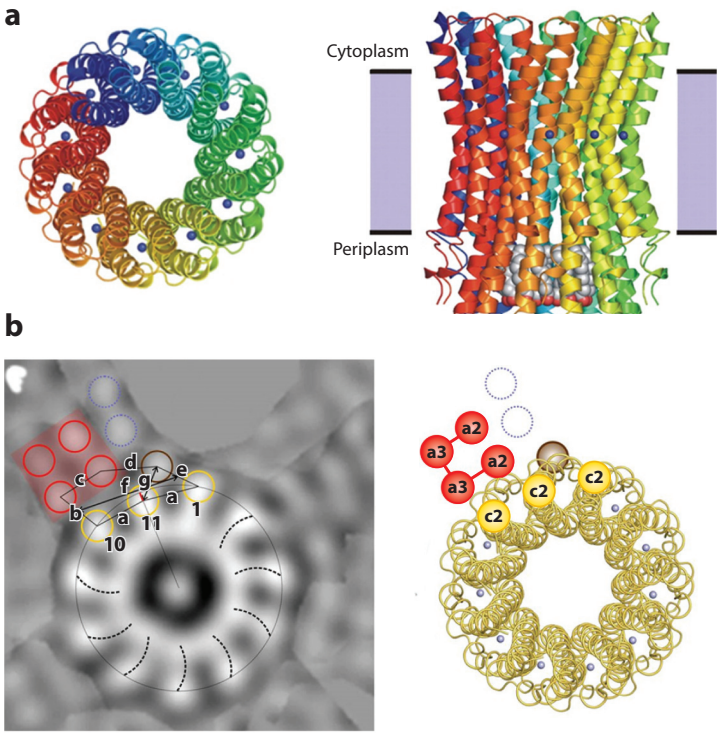

Figure 5

Structural models for F_O. (*a*) Crystal structure of the Na^+-translocating c-ring of *Ilyobacter tartaricus*, with bound Na^+ in the middle of the membrane on each of the hairpin-shaped c-subunits (95). (*b*) Cryo–electron microscopy image of F_O (*left*) and a tentative model for the arrangement of the c_{11}-ring and the transmembrane helices of the a-subunit and perhaps of the b-subunits (*right*) (98).

b_2-subunits (7 Å) has been obtained by cryo–electron microscopy of single F_O molecules from *Ilyobacter tartaricus* (**Figure 5*c*,*d***) (98) and from the related V_O portion of the V-ATP synthase of *Thermus thermophilus* (9.7 Å) (99; for details, see below). The c-ring faces the a-subunit. In *E. coli*, the a-subunit is a four-helix bundle plus one transmembrane helix (TMH). The a-subunit associates with two TMHs of the b-subunits that connect F_O to the top of the $(\alpha\beta)_3$ hexagon of F_1. All three types of subunits are required in order to promote proton conduction by F_O (100).

The c-subunit is highly hydrophobic and is referred to as a proteolipid. Consisting of a hairpin of two TMHs, with a molecular mass of ~8 kDa, the c-subunit carries an ionizable residue (glutamic acid or aspartic acid, depending on the organism) in the middle of the membrane. The pocket around this residue determines the preference of F_O for either H^+ or Na^+ (101). Notably, the Na^+-driven ATP synthase of certain bacteria can operate on H^+ if the Na^+ concentration falls below ~100 μM (see Reference 23 for a review). The wide orifice in the c-ring is probably plugged by phospholipids (102). The copy number of the c-subunit in the ring, *n*, is constant for each species that has been tested. It numbers 8 in bovine mitochondria (103), 10 in yeast mitochondria (96), and 14 in spinach chloroplasts (97, 104), and among bacterial species it varies from 10 (105, 106) to 11 (107), 13 (108, 109), and 15 (110). The copy number is believed to determine the ion-to-ATP ratio, which ranges from 2.67 for $n = 8$ up to 5.00 for $n = 15$. Clearly, organisms that thrive at constant, high PMF (such as mammals) benefit from running at high-speed gear (low *n*), whereas those exposed to variable PMF (such as chloroplasts) and/or low PMF [alkaliphilic

bacteria (109)] benefit from high torque and low-speed gear (high *n*). Meier and colleagues (111) found that several engineered mutations in a conserved stretch of glycines are needed to enlarge the ring size from 11 (wild type) to 12, 13, 14, and more than 14. The relative ease of converting the ring size contrasts with the constant size found within each species. A possible benefit of invariant ring size is that it prevents congeneric individuals from competing in ATP production.

Whereas the symmetry of the c-rings (C_{8-15}) varies between species, the symmetry of F_1 (C_3) does not, virtually excluding the possibility of fine-tuning the detailed reaction steps in one motor to those of the other. Instead, partial reactions in F_O and F_1 are kinetically decoupled from one another by an elastic torque transmission between them (see the section titled Elastic Transmission of Torque, below, and reviews in References 25 and 112).

Design Principle for Rotary, Single-File Ion Transport

Both the ionizable glutamic acid or aspartic acid in the middle of helix 2 of the c-subunit (cG61 in *E. coli*) (113) and the arginine on the a-subunit (aR210 in *E. coli*) (114) are essential for ion translocation by F_O. For this reason, an ion pair is hypothesized to form between adjacent $cD61^-$ and $aR210^+$. With this information at hand, Junge et al. (21) presented a model for rotary ion transport and torque generation by F_O in 1993. Vik & Antonio (115) proposed a similar model. These models are based on three assumptions: (*a*) rotary Brownian fluctuations of the c-ring against the a-subunit; (*b*) electrostatic constraints, namely the obligatory ionization of the very acid residue (in *E. coli*, cD61) that faces the basic residue on the a-subunit (aR210) and the obligatory protonation of the other copies on the c-ring that face the membrane; and (*c*) two staggered access half-channels for ions, left and right of the basic residue on the a-subunit (**Figure 6**) (for an animation, see Related Resources). The width of the fluctuations is limited as long as a given ion pair exists. If an ion hops toward the negative residue through one of the channels, the Coulomb penalty is relieved. The then-neutralized residue on the ring is free to move away from its former partner; that is, the ring may "step forward." The arrival of one ion through one channel is paralleled by the exit of another ion through the other channel, such that a new ion pair is formed with the next copy of the c-subunit on the ring. The staggered access channels, placed left and right of the electropositive residue on the a-subunit, provide chirality to the rotary device. Depending on whether the ion concentration is greater in the phase above or below the membrane, the rotor turns around clockwise or counterclockwise. If torque is applied to the ring, the device pumps ions from one side of the membrane to the other. The interplay between random fluctuations and directed electrochemical force, known as Langevin dynamics, is a common feature of nature's nanomotors (for Berg and colleagues' pioneering work on the flagellar motor, see Reference 116). The quantitative treatment of the F_O motor, which involved solving the Fokker–Planck equation for this model, has revealed its viability in principle (117).

Either residue of the ion pair can be shifted in the plane of the membrane to a neighboring helix of the same subunit (for cD61, see Reference 118; for aR210, see Reference 119) without total loss of the ion transport activity, whereas a perpendicular shift of either one is lethal (120). These observations are compatible with the above functional model.

The direction of rotation, counterclockwise or clockwise, depends on the probability of the ions' presence at either side. In the middle of the membrane, the engine simply counts ions, or in thermodynamic terms, it operates on the entropic component of the electrochemical driving force. The transmembrane voltage as a driving force is invoked by Mitchell's (121) concept of a proton well, in which the two access channels are monospecific for a given ion—say, the proton—and highly conducting (not rate limiting). Each half-channel converts one-half of the transmembrane voltage into its equivalent in terms of the respective local pH (the time-averaged proton activity).

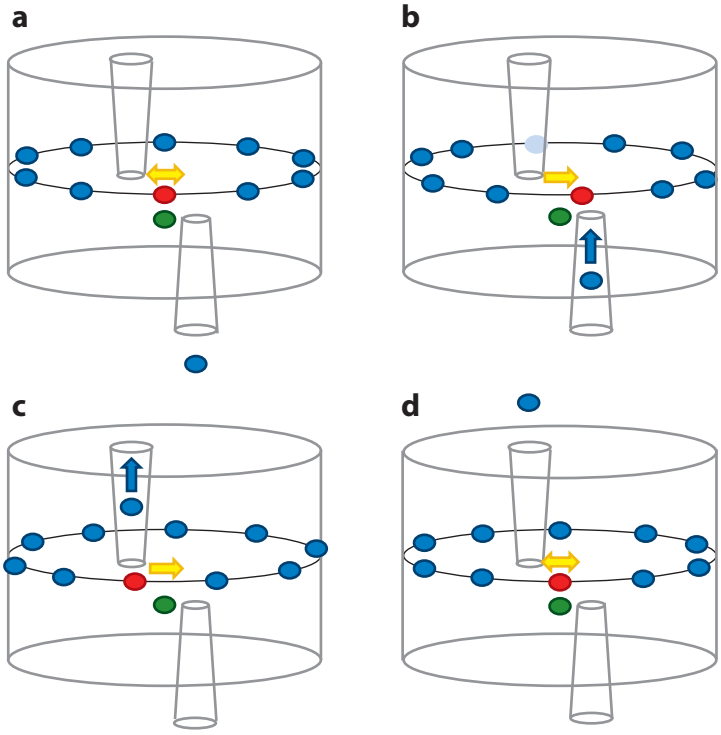

Figure 6

Model of the function of F_O as a torque-generating, single-file ion channel (21). Green, Arg(+); red, Glu(−); blue, GluH.

If the lower phase is more positive by 120 mV than the upper one, it is more positive by 60 mV than the middle of the membrane, and the probability of finding a proton on the right of the ion pair is thus 10-fold greater than in the lower bulk phase; the local pH is more acidic by one unit. By the same argument, the local pH to the left of the ion pair is more alkaline by one unit than that in the upper bulk. This is why such a machine is equally sensitive to the chemical and electric components of the electrochemical driving force across the membrane.

The above discussion refers to the equilibrium state of the rotary ion transporter. In a situation far from equilibrium, that is, under kinetic control, the two components of the driving force are, of course, not a priori equivalent.

The a-Subunit and the Proton Access Channels

Extensive cysteine-mapping studies have revealed that the a-subunit is composed of five TMHs, including a four-helix bundle (see Reference 122 and references therein). At least aTM4, and perhaps aTM5, contacts the c-ring. The former carries the basic residue in *E. coli* aR210. The two copies of the b-subunit, which connects F_O to the upper portion of F_1, are farther away from the c-ring, and they probably contact aTM2 and aTM5. This arrangement of the c_n-, a-, and b_2-subunits, with a rather narrow contact surface between aTM4 and the c-ring of *E. coli* (123), is supported by structural models based on cryo–electron microcopy both for F_O from *Ilyobacter tartaricus*

(98) at 7-Å resolution (**Figure 5*b***) and for the related V_O of the proton-driven V-ATP synthase from *Thermus thermophilus* (99) at 9.7-Å resolution. Subunit I of the latter organism, whose eight TMHs are equivalent to the a-subunit of *E. coli*, makes a surprisingly small contact with the c_{12}-ring. Thus, the two closely apposed access channels for the proton have been tentatively attributed to the narrow contact surface between helices (99). On the basis of extensive cysteine mapping and monitoring of the Ag^+/Cr^+ accessibility of F_O in *E. coli*, Fillingame & Steed (124) have associated the proton half-channel from the p-side with the center of the four-helix bundle. The location of the other half-channel, which connects the acid group on the c-subunit to the n-side, is still controversial. An interface between cTM2 and the a-subunit (124, 125) and an interface between the c-ring and the lipid membrane (126) have been proposed in this role.

Proton Conductance and Assembly

The proton conductance of F_O is too small for detection by the patch-clamp technique. In an initial approach using isolated thylakoids, investigators inferred the electric conductance of F_O from the decay of the transmembrane voltage after excitation of PSII and PSI with a short flash of light. The voltage decay was detected by the intrinsic "molecular voltmeter" in the thylakoid membrane (9, 127). F_1 was detached from the membrane and quantified by immunoassay. The electric conductance per free F_O molecule was calculated to be at least 10 fS (128). A similar estimate was obtained for *E. coli* F_O (129). When calculating the conductance, the authors assumed that every solubilized F_1 left a fully functional F_O in the membrane, an assumption that was not trivial. The uncertainty over the proportion of actually conducting F_O was eventually resolved by a single-molecule-per-vesicle approach (130). One can prepare very small (~30-nm-diameter) chromatophores from *Rhodobacter capsulatus* such that they contain less than one (an average of 0.3) F_OF_1 molecule per vesicle. The proton conductance of one exposed F_OF_1 molecule or, after removal of F_1, of a single F_O molecule is determined via the relaxation of the light-induced voltage pulse. Only one-third of the vesicles show rapid voltage decay, which is attributable to a single exposed F_OF_1 molecule or a single F_O molecule (130). The magnitude of the unitary proton conductance per single F_O molecule is 10 fS (130). The current–voltage relationship is linear; that is, the conductance is ohmic in the range between 7 and 70 mV. There is no evidence for voltage gating of the proton-driven F_O of *Rhodobacter capsulatus* (130), in contrast to claims for sodium-driven F_O (see Reference 131 and references therein). The pH dependence is surprisingly small. With a broad maximum at a pH value of 8, the conductance drops only twofold toward pH values of 6.3 and 10. Also, the hydrogen/deuterium (H/D) kinetic isotope effect, which is 2 at a pH value of 6, vanishes above a pH value of 8.5 (130). This behavior at alkaline pH might indicate proton supply to the rotary channel by water hydrolysis.

The 10-fS conductance corresponds to the translocation of 6,240 protons per second at a 100-mV electric driving force, or twice that, ~12,500 at 200 mV. Thus, the turnover rate of a bacterial c_{10}-ring exceeds 1,000 revolutions per second, ~10 times more than that of the coupled F_OF_1 at the same high driving force (130).

The properties of the rotary proton conduction by F_O—its magnitude of 10 fS, the low pH dependence between 6.5 and 10, and a linear current–voltage relationship—were kinetically modeled with a minimum set of three free parameters (130). The authors of this study assumed that one proton relay group per access channel was in very close proximity to the respective membrane–water interface. If so, each proton relay was exposed to a very small fraction of the transmembrane voltage, giving rise to a linear (ohmic) current–voltage relationship. To account for the shallow

pH dependence, the authors assigned the relay groups very different acid dissociation constants (pKs): one acid (pK 6.5) and the other alkaline (pK 10) (see Reference 130 and references therein). These features of the rotary channel were based solely on kinetic studies, and so far, they lack structural evidence.

During assembly of the holoenzyme from *E. coli*, EF_OF_1, the F_O portion is completed only under the control of F_1 (132). In mutants of *E. coli* with delayed expression of δ-subunit, the stable subcomplexes ab_2 and $c_{10}(\alpha\beta)_3\gamma\varepsilon$ are integrated in the membrane. Their assembly into fully functional EF_OF_1 necessitates the expression of the δ-subunit (133). The δ-subunit connects the b_2-subunit to the crown of $(\alpha\beta)_3$ and couples the rotary proton transfer in F_O to rotary catalysis by F_1. This mode of assembly prevents bare $c_{10}ab_2 = F_O$ from acting as a proton leak.

Rotation of the c-Ring

Rotation of the c-ring, driven by ATP hydrolysis, was first detected in single F_OF_1 molecules (134, 135). The rotary stepping, with steps of 40° and 80°, was dominated by F_1 (65, 66). The expected finer steps of the c-ring in F_O have called for higher resolution of both time and angle. Börsch, Gräber, and their colleagues (136, 137) have relied on FRET between a pair of dyes attached to the rotor and the stator, a method that is also applicable to membrane-bound F_OF_1, whether driven by ATP hydrolysis or PMF. Thirty-six-degree steps of the c_{10}-ring from *E. coli* were detected at the limits of resolution (138).

Frasch and colleagues (70, 139) chose another approach. They attached gold nanorods to the c_{10}-ring of immobilized F_OF_1 from *E. coli* and recorded the orientation-dependent color changes of the back-scattered light. Because of the small size of the rods, the rotation was not limited by viscosity, and it revealed the intrinsic substepping of the c-ring in F_O. These steps were superimposed onto those of the driving motor, F_1.

Modeling F_O Dynamics

Several research groups have extended this phenomenological scheme for rotary single-file ion conduction by F_O to explicitly incorporate further structural features of c_nab_2. All these attempts have suffered from the lack of a detailed structural model of this ensemble. One team proposed a tentative energy landscape and simulated rotary trajectories by Langevin dynamics (131, 140); however, how the landscape relates to actual structural details is unclear. Two other groups used available structural information about the c-ring to carry out coarse-grained MD simulations (141, 142). When starting from a position where the ion pair ($cAsp^-/aArg^+$) is perfectly aligned, the energy profile to the right and the left of this position is asymmetric. It explains one rotational step but not the continuous rotation. Continuous rotation requires two staggered half-channels for ion access, which create chirality (21). More recently, Mukherjee & Warshel (143) used a coarse-grained approach to model both F_O rotation and proton transfer across the membrane. They calculated an (electrostatic) energy landscape based on the limited available structural information about the c_na moiety. They assumed two staggered half-channels used by the proton to access the essential anionic residue from either side of the membrane. By solving the statistical dynamics of proton motion and ring rotation over this energy profile, Mukherjee & Warshel (143) obtained a typical proton transfer rate of 42,000 H^+ ions per second at a pH value of 8 (on both sides of the membrane) and an electric driving force of 200 mV. The order of magnitude compares well with the experimentally determined 12,500 H^+ ions per second (130), considering the ambiguity of certain structural features and the sensitivity of kinetic constants to small differences in energy landscape.

F_OF_1, THE PROTON-DRIVEN ATP SYNTHASE

Two Coupled Rotary Motors

In the holoenzyme F_OF_1, two motors operate against each other. Net turnover stops when the thermodynamic driving forces are equal (Equation 1*a*). If the PMF prevails, then the enzyme synthesizes ATP, and if the molar free energy of ATP hydrolysis prevails, then the enzyme pumps protons and generates PMF. This simple picture holds if two conditions are met: (*a*) perfect coupling of the two motors and (*b*) full reversibility of the enzyme. The rotation of the c-ring is mechanically coupled to the turnover of the F_1-ATPase (90), and there is no leak conductance (i.e., proton slip) if the nucleotide concentrations are greater than 1 μM (91, 92). Various means of regulation, however, may convert the microscopically reversible enzyme into a seemingly irreversible device (see the section titled Regulation, below).

For a perfectly coupled dual motor, one expects the ratio of protons transported over ATP processed (the ratio of H^+ to ATP) to be determined by the ratio of the copy number of the c-subunit in the F_O ring to the number of catalytic sites in F_1, which is 3 in all organisms. For the chloroplast enzyme, which has 14 copies of the c-subunit, the ratio should be 14 to 3, or 4.7. Why this expectation has not been met in kinetic and thermodynamic experiments despite considerable efforts is an open question (see Reference 144 and references therein). Instead of 4.7, a ratio of 4 has been consistently observed—this result implies "overcoupling," which cannot exist.

Elastic Transmission of Torque

Circumstantial evidence suggests that the detailed reaction steps in F_O are kinetically decoupled from those in F_1. Examples are the significant size variation of the c-ring (ranging from 8 to 15 copies) in different organisms and the functionality of a chimeric construct composed of the Na^+-translocating F_O of *P. modestum* and the F_1 of *E. coli* (145). Hypotheses that kinetic decoupling occurs by elastic torque transmission between F_O and F_1 (146, 147) were ultimately proven correct by single-molecule experiments with F_OF_1 from *E. coli*, in which the torque generated by F_1 and transmitted to F_O was measured via the curvature of a 3-μm-long actin filament (90). Although torque production by F_1 was expected to have three steps (under the given conditions), the torque output to the actin filament on F_O was almost constant (90). This surprising observation can be explained by solving the Fokker–Planck equation of a stepping nanomotor that is elastically coupled to a heavy load (90). Increasing the compliance of the elastic buffer has two consequences: a flattening of the torque profile at the output and an increase of the turnover rate under load. The latter effect is rather dramatic (**Figure 7*b***). An elastic buffer increases the turnover rate by orders of magnitude over the rate obtained with a stiff transmission between motor and load. This benefit of a compliant transmission likewise applies to all of nature's intrinsically stepping nanomotors that drive a heavy load.

The distribution of compliant and stiff domains over F_OF_1 was determined by a fluctuation analysis under selective stiffening by use of engineered disulfide bridges (65, 148). Broadly speaking, the most compliant domain in F_OF_1 (with a torsion spring constant of 70 pN·nm) is at the interface of F_O and F_1 and involves the foot of the γ-subunit plus the ε-subunit [and perhaps the c-ring (149)] (**Figure 7*a***). The C-terminal hinge of the β-subunits (with a stiffness of ∼70 pN·nm) adds further compliance such that the total spring constant is ∼35 pN·nm (see Reference 25 and references therein). Other domains of *E. coli* F_OF_1 that are very stiff include the portion of the γ-subunit between the hinge and the C terminus (700 pN·nm) and the eccentric stator [1,500 pN·nm, involving the b-subunit (148)]. One fluctuation experiment (65) was simulated by MD

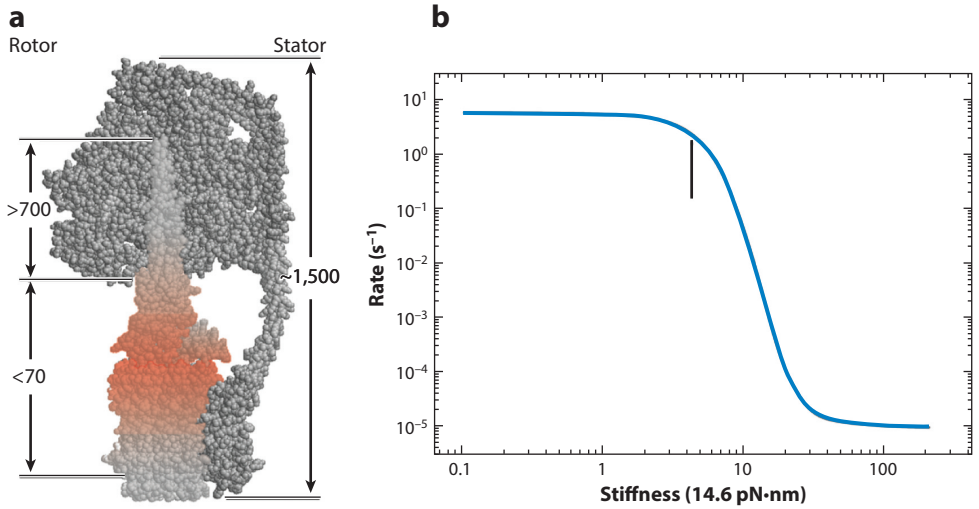

Figure 7

The elastic torque transmission between the two rotary motors in F_OF_1. (*a*) Distribution of stiff (*gray*) and compliant (*pink*) domains over the homology structure of *Escherichia coli* F_OF_1. Numbers indicate the torsion spring constants in piconewton nanometers (65, 148). (*b*) Calculated turnover rate of a nanosized stepper motor being elastically coupled to a heavy viscous load as a function of the torsion spring constant between motor and load (90).

(150). The magnitude of the torsion stiffness of the γ-subunit between the C-terminal end and its contact area with the hinge on the β-subunit, 700 N·m, matched the experimentally determined figure. It may be difficult to accept that similar values result from two approaches addressing such different timescales, namely milliseconds in the experiment (65) and nanoseconds in the simulation (150). The reason for the equivalent values is the scaling of the viscous drag and, therefore, the rotational fluctuation time by the third power of the probe length (100 nm in the former approach and 1 nm in the latter).

The Enzyme in the Coupling Membrane

F_OF_1 is monomeric in the coupling membranes of photosynthetic organisms. In contrast, in mammalian mitochondria it forms bands of dimers lining the rim of cristae. The correlation time of rotational diffusion of F_OF_1 in the thylakoid membrane of chloroplasts [~100 μs (53)] is approximately one-tenth as long as the rotation period of the c-ring in F_O (~1 ms) at high driving force (130). This observation implies that viscous drag of the lipid matrix on the rotating c-ring is small. The rate of proton-driven rotation of the c-ring in bare F_O is much faster (~1,000 revolutions per second) than when it is coupled to F_1 in the holoenzyme (100 revolutions per second). Thus, the proton transporting c-ring rapidly equilibrates with the elastic buffer, which provides F_1 with torque when needed for the reactive stepping of ATP synthesis.

Solitary F_OF_1 molecules are located at the top and bottom plates of grana stacks and on stroma lamellae. The generators of PMF (e.g., PSII) may be a distance of several hundred nanometers from the consumer, F_OF_1. Under steady turnover of the proton pumps and the proton-translocating ATP synthase, lateral losses of PMF are inevitable. The two components of the PMF propagate with different velocities along the membrane. A locally generated voltage pulse propagates fast and practically loss free because of the high electric conductance on both sides of the membrane.

As mentioned above, the whole thylakoid system, which contains ~10^8 chlorophyll and 10^5 F_OF_1 molecules, may be considered electrically isopotential (30). The propagation of the chemical driving force, however, is slow and not loss free. The proton is a minority charge carrier, and its motion is electrically compensated by other ions. Protons diffuse from proton pumps to the ATP synthase at the p-side of the membrane and back at the n-side (**Figure 1*b***). The driving force of proton diffusion between sources and sinks is a lateral ΔpH difference. As a consequence, there is a lateral loss of the transmembrane ΔpH difference between the pumps and F_OF_1. The magnitude of this loss of PMF was recently determined in active mitochondria (151), in which F_OF_1 dimers line the rim of disk-shaped cristae and the cytochrome oxidase (a proton pump) resides in the flat portions. The lateral drop of the transmembrane ΔpH slightly modifies Mitchell's original concept (5). Further modifications have been discussed, namely enhanced diffusion of the proton along the surface of the membrane and their delayed escape from the membrane surface into the adjacent bulk phase. Although there has been no experimental evidence for enhanced surface diffusion, the delayed escape of protons from the surface has been established (152) and may be important in enabling alkaliphilic bacteria to synthesize ATP at a seemingly too-low bulk-to-bulk PMF (19). In the narrow gap between thylakoid membranes, the terms surface and bulk lose their distinction. For protons, the bulk phase is defined more by buffering groups at the surface than by aqueous volume. Nevertheless, any charge crossing the dielectric membrane via F_OF_1 can be detected as a proton entering from the p-surface and leaving from the n-surface of the thylakoid membrane (153).

Regulation

In cyanobacteria, ATP synthase shares a coupling membrane with the electron transport chains of both photosynthesis and respiration. Whether generated in light or dark or under aerobic or anaerobic conditions, ATP molecules are powered by the PMF. In higher plants, photosynthesis and respiration are segregated from each other, the former in the thylakoid membrane of chloroplasts and the latter in the crista membrane of mitochondria. To prevent futile hydrolysis by the chloroplast enzyme of ATP made by mitochondria, the chloroplast enzyme is downregulated in the dark. Under oxidizing conditions, enzyme activity stops before the PMF drops below the thermodynamic compensation point. The apparent irreversibility of the auto-oxidized enzyme holds regardless of whether the electric component ($F \cdot \Delta\varphi$) (10) or the chemical component ($-2.3 \cdot RT \cdot \Delta$pH) of the PMF is dominant (154). Whereas ATP hydrolysis is blocked at low PMF in the oxidized enzyme, at high PMF ATP synthesis proceeds at a high rate (155). The inhibition of ATP hydrolysis is relieved under illumination, when photosynthetic electron transport provides reducing equivalents. Chloroplast F_OF_1 is thiol-activated by thioredoxin (156). Two cysteine residues in the foot of the chloroplast γ-subunit are the target of modulation. They are absent in the cyanobacterial wild-type enzyme (157) and in the enzymes of *Bacillus* PS3, other α-bacteria, and mitochondria. If the regulatory stretch of the chloroplast γ-subunit is engineered into $(\alpha\beta)_3\gamma$ from *Bacillus* PS3, its ATPase activity is enhanced upon reduction (158). In single-molecule experiments, longer pauses of rotation are observed if $(\alpha\beta)_3\gamma$ is oxidized (159). In addition to the two actuators ($\Delta\varphi$ and ΔpH) and the modulator pair (thioredoxin/dioxygen), further factors are involved in the activity regulation, namely tightly bound ADP and the ε-subunit. How these factors interact to prevent futile ATP hydrolysis in the chloroplast enzyme is the subject of active research (see Reference 160 and references therein). When relieving the inhibition, the actuator, PMF, is probably mechanically sensed via the directionality of F_O-induced rotation and/or the magnitude of torque, rather than electrostatically by a group of gating charges, as in cation channels (161).

Mammalian mitochondria host a special inhibitor protein of F-ATPase (162), known as IF_1. Whereas IF_1 inhibits ATP hydrolysis, it does not inhibit synthesis (163). The structural mechanisms underlying this unidirectional action have recently been determined (164). On the basis of crystal structures of the mitochondrial F-ATPase, with one, two, and three bound molecules of an N-terminal fragment of the inhibitor, investigators have proposed that, in solution, an unordered segment binds to the cleft in $(\alpha\beta)_E$. This segment is then sequentially structured into an α-helical shape and is more deeply incorporated between the γ-subunit and $(\alpha\beta)_3$ during the subsequent 120° steps. It then blocks the rotation of the central shaft. Reversal of the direction of rotation, as under proton-driven ATP synthesis, sequentially expels the inhibitor into the medium. The obvious physiological role of IF_1 is to prevent mitochondria from hydrolyzing ATP when the PMF is low (e.g., during anoxia). It may also play a role in preventing apoptosis, in particular in tumor cells (see Reference 164 and references therein).

EPILOGUE

ATP synthase (F_OF_1-ATPase of F-ATPase) operates by the same electromechanochemical mechanism in numerous organisms, regardless of their evolutionary history and habitat. Its remote relatives, archaeal A-ATPase and eukaryotic vacuolar V-ATPase, probably operate by the same principle. They probably evolved from a common ancestor (81, 165). One difference between F-ATPase and V-ATPase is the ion-translocating ring in F_O and V_O. In the V-ATPase from yeast, each copy on the ring in V_O contains four transmembrane helices (versus two in F_O) and one or two negative charges in the middle of the membrane. Given an elastic torque transmission that is similar to that established for F-ATPase, this structural difference must not affect the efficient cooperation between the two rotary nanomotors of V-ATPase. V-ATPase operates as an ATP-driven proton pump in the plasma membrane of eukaryotic cells and in internal organelles such as vacuoles, lysosomes, synaptic vesicles, endosomes, secretory granules, and the Golgi apparatus, in which it can produce an internal pH lower than one. The tissue-specific regulation of V-ATPase in eukaryotes is a subject of great biomedical interest that calls for similarly detailed structural and kinetic data, as are available for F-ATPase.

DISCLOSURE STATEMENT

The authors are not aware of any affiliations, memberships, funding, or financial holdings that might be perceived as affecting the objectivity of this review.

ACKNOWLEDGMENTS

The authors apologize to all the investigators whose work could not be cited in this review. W.J. thanks his coworkers over many years, in particular Siegfried Engelbrecht (who is also acknowledged for his help with **Figure 2**), and acknowledges financial support from the Lower Saxony Ministry of Science and the Volkswagen Foundation.

LITERATURE CITED

1. Blankenship RE, Tiede DM, Barber J, Brudvig GW, Fleming G, et al. 2011. Comparing photosynthetic and photovoltaic efficiencies and recognizing the potential for improvement. *Science* 332:805–9
2. Nelson N, Junge W. 2015. Structure and energy transfer in photosystems of oxygenic photosynthesis. *Annu. Rev. Biochem.* 84:659–83

3. Pullman ME, Penefsky H, Racker E. 1958. A soluble protein fraction required for coupling phosphorylation to oxidation in submitochondrial fragments of beef heart mitochondria. *Arch. Biochem. Biophys.* 76:227–30
4. Mitchell P. 1961. Coupling of photophosphorylation to electron and hydrogen transfer by a chemiosmotic type of mechanism. *Nature* 191:144–48
5. Mitchell P. 1966. Chemiosmotic coupling in oxidative and photosynthetic phosphorylation. *Physiol. Rev.* 41:445–502
6. Cruz JA, Sacksteder CA, Kanazawa A, Kramer DM. 2001. Contribution of electric field ($\Delta\Psi$) to steady-state transthylakoid proton motive force (*pmf*) in vitro and in vivo. Control of *pmf* parsing into $\Delta\Psi$ and ΔpH by ionic strength. *Biochemistry* 40:1226–37
7. Takizawa K, Cruz JA, Kanazawa A, Kramer DM. 2007. The thylakoid proton motive force in vivo. Quantitative, non-invasive probes, energetics, and regulatory consequences of light-induced PMF. *Biochim. Biophys. Acta* 1767:1233–44
8. Jagendorf AT, Uribe E. 1966. ATP formation caused by acid–base transition of spinach chloroplast. *PNAS* 55:170–77
9. Junge W, Witt HT. 1968. On the ion transport system of photosynthesis. Investigation on a molecular level. *Z. Naturforsch.* 23B:244–54
10. Junge W, Rumberg B, Schroeder H. 1970. Necessity of an electric potential difference and its use for photophosphorylation in short flash groups. *Eur. J. Biochem.* 14:575–81
11. Boyer PD, Chance B, Ernster L, Mitchell P, Racker E, Slater EC. 1977. Oxidative phosphorylation and photophosphorylation. *Annu. Rev. Biochem.* 46:955–1026
12. Kayalar C, Rosing J, Boyer PD. 1977. An alternating site sequence for oxidative phosphorylation suggested by measurement of substrate binding patterns and exchange reaction inhibitions. *J. Biol. Chem.* 252:2486–91
13. Boyer PD. 1977. Conformational coupling in oxidative phosphorylation and photophosphorylation. *Trends Biochem. Sci.* 2:38–41
14. Boyer PD, Kohlbrenner WE. 1981. The present status of the binding-change mechanism and its relation to ATP formation by chloroplasts. In *Energy Coupling in Photosynthesis*, ed. BR Selman, S Selman-Reimer, pp. 231–41. Amsterdam: Elsevier
15. Rao R, Senior AE. 1987. The properties of hybrid F_1-ATPase enzymes suggest that a cyclical catalytic mechanism involving three catalytic sites occurs. *J. Biol. Chem.* 25:17450–54
16. Cross RL, Nalin CM. 1982. Adenine nucleotide binding sites on beef heart F_1-ATPase. Evidence for three exchangeable sites that are distinct from three noncatalytic sites. *J. Biol. Chem.* 257:2874–81
17. Weber J, Wilke-Mounts S, Senior AE. 1994. Cooperativity and stoichiometry of substrate binding to the catalytic sites of *Escherichia coli* F_1-ATPase. Effects of magnesium, inhibitors, and mutation. *J. Biol. Chem.* 269:20462–67
18. Walker JE, Fearnely IM, Gay NJ, Gibson BW, Northrop FD, et al. 1985. Primary structure and subunit stoichiometry of F_1-ATPase from bovine mitochondria. *J. Mol. Biol.* 184:677–701
19. Junge W. 2013. Half a century of molecular bioenergetics. *Biochem. Soc. Trans.* 41:1207–18
20. Boyer PD. 1997. The ATP synthase—a splendid molecular machine. *Annu. Rev. Biochem.* 66:717–49
21. Junge W, Lill H, Engelbrecht S. 1997. ATP synthase: an electrochemical transducer with rotatory mechanics. *Trends Biochem. Sci.* 22:420–23
22. Kinosita K Jr, Adachi K, Itoh H. 2004. Rotation of F_1-ATPase: how an ATP-driven molecular machine may work. *Annu. Rev. Biophys. Biomol. Struct.* 33:245–68
23. von Ballmoos C, Wiedenmann A, Dimroth P. 2009. Essentials for ATP synthesis by F_1F_O ATP synthases. *Annu. Rev. Biochem.* 78:649–72
24. Walker JE. 2013. The ATP synthase: the understood, the uncertain and the unknown. *Biochem. Soc. Trans.* 41:1–16
25. Junge W, Sielaff H, Engelbrecht S. 2009. Torque generation and elastic power transmission in the rotary F_OF_1-ATPase 3. *Nature* 459:364–70
26. Schliephake W, Junge W, Witt HT. 1968. Correlation between field formation, proton translocation, and the light reactions in photosynthesis. *Z. Naturforsch.* 23:1571–78

27. Hope AB, Rich PR. 1989. Proton uptake by the chloroplast cytochrome *bf* complex. *Biochim. Biophys. Acta* 975:96–103
28. Stolz B, Walz D. 1988. The absorption spectrum of single blebs and the specific surface of thylakoids. *Mol. Cell. Biol.* 7:83–88
29. Menke W. 1962. Structure and chemistry of plastids. *Annu. Rev. Plant Physiol.* 13:27–44
30. Schönknecht G, Althoff G, Junge W. 1990. The electric unit size of thylakoid membranes. *FEBS Lett.* 277:65–68
31. Paolillo DJ Jr. 1970. The three-dimensional arrangement of intergranal lamellae in chloroplasts. *J. Cell Sci.* 6:243–55
32. Mustardy L, Buttle K, Steinbach G, Garab G. 2008. The three-dimensional network of the thylakoid membranes in plants: quasihelical model of the granum–stroma assembly. *Plant Cell* 20:2552–57
33. Austin JR 2nd, Staehelin LA. 2011. Three-dimensional architecture of grana and stroma thylakoids of higher plants as determined by electron tomography. *Plant Physiol.* 155:1601–11
34. Daum B, Kühlbrandt W. 2011. Electron tomography of plant thylakoid membranes. *J. Exp. Bot.* 62:2393–402
35. Andersson B, Anderson JM. 1980. Lateral heterogeneity in the distribution of chlorophyll–protein complexes of the thylakoid membranes of spinach chloroplasts. *Biochim. Biophys. Acta* 593:427–40
36. Staehelin LA. 1975. Chloroplast membrane structure. Intramembranous particles of different sizes make contact in stacked membrane regions. *Biochim. Biophys. Acta* 408:1–11
37. Daum B, Nicastro D, Austin J, McIntosh JR, Kühlbrandt W. 2010. Arrangement of photosystem II and ATP synthase in chloroplast membranes of spinach and pea. *Plant Cell* 22:1299–312
38. Albertsson P. 2001. A quantitative model of the domain structure of the photosynthetic membrane. *Trends Plant Sci.* 6:349–58
39. Trissl HW, Wilhelm C. 1993. Why do thylakoid membranes from higher plants form grana stacks? *Trends Biochem. Sci.* 18:415–19
40. Anderson JM, Andersson B. 1988. The dynamic photosynthetic membrane and regulation of solar energy conversion. *Trends Biochem. Sci.* 13:351–55
41. Abrahams JP, Leslie AG, Lutter R, Walker JE. 1994. The structure of F_1-ATPase from bovine heart mitochondria determined at 2.8 Å resolution. *Nature* 370:621–28
42. Bowler MW, Montgomery MG, Leslie AG, Walker JE. 2007. Ground state structure of F_1-ATPase from bovine heart mitochondria at 1.9 Å resolution. *J. Biol. Chem.* 282:14238–42
43. Walker JE, Saraste M, Gay NJ. 1982. *E. coli* F_1-ATPase interacts with a membrane protein component of a proton channel. *Nature* 298:867–69
44. Kötting C, Blessenohl M, Suveyzdis Y, Goody RS, Wittinghofer A, Gerwert K. 2006. A phosphoryl transfer intermediate in the GTPase reaction of Ras in complex with its GTPase-activating protein. *PNAS* 103:13911–16
45. Menz RI, Walker JE, Leslie AG. 2001. Structure of bovine mitochondrial F_1-ATPase with nucleotide bound to all three catalytic sites: implications for the mechanism of rotary catalysis. *Cell* 106:331–41
46. Rees DM, Montgomery MG, Leslie AG, Walker JE. 2012. Structural evidence of a new catalytic intermediate in the pathway of ATP hydrolysis by F_1-ATPase from bovine heart mitochondria. *PNAS* 109:11139–43
47. Groth G, Pohl E. 2001. The structure of the chloroplast F_1-ATPase at 3.2 Å resolution. *J. Biol. Chem.* 276:1345–52
48. Stocker A, Keis S, Vonck J, Cook GM, Dimroth P. 2007. The structural basis for unidirectional rotation of thermoalkaliphilic F_1-ATPase. *Structure* 15:904–14
49. Kabaleeswaran V, Shen H, Symersky J, Walker JE, Leslie AG, Mueller DM. 2009. Asymmetric structure of the yeast F_1-ATPase in the absence of bound nucleotides. *J. Biol. Chem.* 284:10546–51
50. Cingolani G, Duncan TM. 2011. Structure of the ATP synthase catalytic complex (F_1) from *Escherichia coli* in an autoinhibited conformation. *Nat. Struct. Mol. Biol.* 18:701–7
51. Duncan TM, Bulygin VV, Zhou Y, Hutcheon ML, Cross RL. 1995. Rotation of subunits during catalysis by *Escherichia coli* F_1-ATPase. *PNAS* 92:10964–68
52. Sabbert D, Engelbrecht S, Junge W. 1996. Intersubunit rotation in active F-ATPase. *Nature* 381:623–25

53. Sabbert D, Engelbrecht S, Junge W. 1997. Functional and idling rotatory motion within F_1-ATPase. *PNAS* 94:4401–5
54. Noji H, Yasuda R, Yoshida M, Kinosita K. 1997. Direct observation of the rotation of F-ATPase. *Nature* 386:299–302
55. Yasuda R, Noji H, Yoshida M, Kinosita K Jr, Itoh H. 2001. Resolution of distinct rotational substeps by submillisecond kinetic analysis of F_1-ATPase. *Nature* 410:898–904
56. Shimabukuro K, Yasuda R, Muneyuki E, Hara KY, Kinosita K Jr, Yoshida M. 2003. Catalysis and rotation of F_1 motor: Cleavage of ATP at the catalytic site occurs in 1 ms before 40 degree substep rotation. *PNAS* 100:14731–36
57. Ueno H, Suzuki T, Kinosita K, Jr, Yoshida M. 2005. ATP-driven stepwise rotation of F_OF_1-ATP synthase. *PNAS* 102:1333–38
58. Adachi K, Oiwa K, Nishizaka T, Furuike S, Noji H, et al. 2007. Coupling of rotation and catalysis in F_1-ATPase revealed by single-molecule imaging and manipulation. *Cell* 130:309–21
59. Masaike T, Koyama-Horibe F, Oiwa K, Yoshida M, Nishizaka T. 2008. Cooperative three-step motions in catalytic subunits of F_1-ATPase correlate with 80 degrees and 40 degrees substep rotations. *Nat. Struct. Mol. Biol.* 15:1326–33
60. Sekiya M, Hosokawa H, Nakanishi-Matsui M, Al-Shawi MK, Nakamoto RK, Futai M. 2010. Single molecule behavior of inhibited and active states of *Escherichia coli* ATP synthase F_1 rotation. *J. Biol. Chem.* 285:42058–67
61. Watanabe R, Iino R, Noji H. 2010. Phosphate release in F_1-ATPase catalytic cycle follows ADP release. *Nat. Chem. Biol.* 6:814–20
62. Watanabe R, Noji H. 2014. Characterization of the temperature-sensitive reaction of F_1-ATPase by using single-molecule manipulation. *Sci. Rep.* 4:4962
63. Noji H, Häsler K, Junge W, Kinosita K, Yoshida M, Engelbrecht S. 1999. Rotation of *Escherichia coli* F_1-ATPase. *Biochem. Biophys. Res. Commun.* 260:597–99
64. Bilyard T, Nakanishi-Matsui M, Steel BC, Pilizota T, Nord AL, et al. 2013. High-resolution single-molecule characterization of the enzymatic states in *Escherichia coli* F_1-ATPase. *Philos. Trans. R. Soc. Lond. B* 368:20120023
65. Sielaff H, Rennekamp H, Wächter A, Xie H, Hilbers F, et al. 2008. Domain compliance and elastic power transmission in rotary F_OF_1-ATPase. *PNAS* 105:17760–65
66. Sielaff H, Rennekamp H, Engelbrecht S, Junge W. 2008. Functional halt positions of rotary F_OF_1-ATPase correlated with crystal structures. *Biophys. J.* 95:4979–87
67. Suzuki T, Tanaka K, Wakabayashi C, Furuike S, Saita E, et al. 2014. Chemo-mechanical coupling of human mitochondrial F_1-ATPase motor. *Nat. Chem. Biol.* 10:930–36
68. York J, Spetzler D, Hornung T, Ishmukhametov R, Martin J, Frasch WD. 2007. Abundance of *Escherichia coli* F_1-ATPase molecules observed to rotate via single-molecule microscopy with gold nanorod probes. *J. Bioenerg. Biomembr.* 39:435–39
69. Hornung T, Martin J, Spetzler D, Ishmukhametov R, Frasch WD. 2011. Microsecond resolution of single-molecule rotation catalyzed by molecular motors. *Methods Mol. Biol.* 778:273–89
70. Martin JL, Ishmukhametov R, Hornung T, Ahmad Z, Frasch WD. 2014. Anatomy of F_1-ATPase powered rotation. *PNAS* 111:3715–20
71. Okuno D, Fujisawa R, Iino R, Hirono-Hara Y, Imamura H, Noji H. 2008. Correlation between the conformational states of F_1-ATPase as determined from its crystal structure and single-molecule rotation 1. *PNAS* 105:20722–27
72. Shimo-Kon R, Muneyuki E, Sakai H, Adachi K, Yoshida M, Kinosita K Jr. 2010. Chemo-mechanical coupling in F_1-ATPase revealed by catalytic site occupancy during catalysis. *Biophys. J.* 98:1227–36
73. Kabaleeswaran V, Puri N, Walker JE, Leslie AG, Mueller DM. 2006. Novel features of the rotary catalytic mechanism revealed in the structure of yeast F_1-ATPase. *EMBO J.* 25:5433–42
74. Okazaki K, Hummer G. 2013. Phosphate release coupled to rotary motion of F_1-ATPase. *PNAS* 110:16468–73
75. Weber J, Wilke-Mounts S, Lee RSF, Grell E, Senior AE. 1993. Specific placement of tryptophan in the catalytic sites of *Escherichia coli* F_1-ATPase provides a direct probe of nucleotide binding: Maximal ATP hydrolysis occurs with three sites occupied. *J. Biol. Chem.* 268:20126–33

76. Weber J, Bowman C, Senior AE. 1996. Specific tryptophan substitution in catalytic sites of *Escherichia coli* F_1-ATPase allows differentiation between bound substrate ATP and product ADP in steady-state catalysis. *J. Biol. Chem.* 271:18711–18
77. Nishizaka T, Oiwa K, Noji H, Kimura S, Muneyuki E, et al. 2004. Chemomechanical coupling in F_1-ATPase revealed by simultaneous observation of nucleotide kinetics and rotation. *Nat. Struct. Mol. Biol.* 11:142–48
78. Itoh H, Takahashi A, Adachi K, Noji H, Yasuda R, et al. 2004. Mechanically driven ATP synthesis by F_1-ATPase. *Nature* 427:465–68
79. Rondelez Y, Tresset G, Nakashima T, Kato-Yamada Y, Fujita H, et al. 2005. Highly coupled ATP synthesis by F_1-ATPase single molecules. *Nature* 433:773–77
80. Uchihashi T, Iino R, Ando T, Noji H. 2011. High-speed atomic force microscopy reveals rotary catalysis of rotorless F_1-ATPase. *Science* 333:755–58
81. Mulkidjanian AY, Makarova KS, Galperin MY, Koonin EV. 2007. Inventing the dynamo machine: the evolution of the F-type and V-type ATPases. *Nat. Rev. Microbiol.* 5:892–99
82. Müller M, Pänke O, Junge W, Engelbrecht S. 2002. F_1-ATPase, the C-terminal end of subunit γ, is not required for ATP hydrolysis–driven rotation. *J. Biol. Chem.* 277:23308–13
83. Hossain MD, Furuike S, Maki Y, Adachi K, Suzuki T, et al. 2008. Neither helix in the coiled coil region of the axle of F_1-ATPase plays a significant role in torque production. *Biophys. J.* 95:4837–44
84. Kohori A, Chiwata R, Hossain MD, Furuike S, Shiroguchi K, et al. 2011. Torque generation in F_1-ATPase devoid of the entire amino-terminal helix of the rotor that fills half of the stator orifice. *Biophys. J.* 101:188–95
85. Usukura E, Suzuki T, Furuike S, Soga N, Saita E, et al. 2012. Torque generation and utilization in motor enzyme F_OF_1-ATP synthase: half-torque F_1 with short-sized pushrod helix and reduced ATP synthesis by half-torque F_OF_1. *J. Biol. Chem.* 287:1884–91
86. Chiwata R, Kohori A, Kawakami T, Shiroguchi K, Furuike S, et al. 2014. None of the rotor residues of F_1-ATPase are essential for torque generation. *Biophys. J.* 106:2166–74
87. Czub J, Grubmüller H. 2014. Rotation triggers nucleotide-independent conformational transition of the empty β subunit of F_1-ATPase. *J. Am. Chem. Soc.* 136:6960–68
88. Wang H, Oster G. 1998. Energy transduction in the F_1 motor of ATP synthase. *Nature* 396:279–82
89. Cherepanov DA, Junge W. 2001. Viscoelastic dynamics of actin filaments coupled to rotary F-ATPase: curvature as an indicator of the torque. *Biophys. J.* 81:1234–44
90. Pänke O, Cherepanov DA, Gumbiowski K, Engelbrecht S, Junge W. 2001. Viscoelastic dynamics of actin filaments coupled to rotary F-ATPase: torque profile of the enzyme. *Biophys. J.* 81:1220–33
91. Feniouk BA, Mulkidjanian AY, Junge W. 2005. Proton slip in the ATP synthase of *Rhodobacter capsulatus*: induction, proton conduction, and nucleotide dependence. *Biochim. Biophys. Acta* 1706:184–94
92. Groth G, Junge W. 1993. Proton slip of chloroplast ATPase: its nucleotide dependence, energetic threshold and relation to an alternating site mechanism of catalysis. *Biochemistry* 32:8103–11
93. Mukherjee S, Warshel A. 2011. Electrostatic origin of the mechanochemical rotary mechanism and the catalytic dwell of F_1-ATPase. *PNAS* 108:20550–55
94. Pu J, Karplus M. 2008. How subunit coupling produces the γ-subunit rotary motion in F_1-ATPase. *PNAS* 105:1192–97
95. Meier T, Polzer P, Diederichs K, Welte W, Dimroth P. 2005. Structure of the rotor ring of F-type Na^+-ATPase from *Ilyobacter tartaricus*. *Science* 308:659–62
96. Stock D, Leslie AG, Walker JE. 1999. Molecular architecture of the rotary motor in ATP synthase. *Science* 286:1700–5
97. Vollmar M, Schlieper D, Winn M, Buchner C, Groth G. 2009. Structure of the c14 rotor ring of the proton translocating chloroplast ATP synthase. *J. Biol. Chem.* 284:18228–35
98. Hakulinen JK, Klyszejko AL, Hoffmann J, Eckhardt-Strelau L, Brutschy B, et al. 2012. Structural study on the architecture of the bacterial ATP synthase F_O motor. *PNAS* 109:e2050–56
99. Lau WC, Rubinstein JL. 2012. Subnanometre-resolution structure of the intact *Thermus thermophilus* H^+-driven ATP synthase. *Nature* 481:214–18
100. Schneider E, Altendorf K. 1985. All three subunits are required for the reconstitution of an active proton channel (F_O) of *Escherichia coli* ATP synthase (F_1F_O). *EMBO J.* 4:515–18

101. Preiss L, Yildiz O, Hicks DB, Krulwich TA, Meier T. 2010. A new type of proton coordination in an F_1F_O-ATP synthase rotor ring. *PLOS Biol.* 8:e1000443
102. Meier T, Matthey U, Henzen F, Dimroth P, Müller DJ. 2001. The central plug in the reconstituted undecameric cylinder of a bacterial ATP synthase consists of phospholipids. *FEBS Lett.* 505:353–56
103. Watt IN, Montgomery MG, Runswick MJ, Leslie AG, Walker JE. 2010. Bioenergetic cost of making an adenosine triphosphate molecule in animal mitochondria. *PNAS* 107:16823–27
104. Seelert H, Poetsch A, Dencher NA, Engel A, Stahlberg H, Müller DJ. 2000. Proton-powered turbine of a plant motor. *Nature* 405:418–19
105. Jiang W, Hermolin J, Fillingame RH. 2001. The preferred stoichiometry of c subunits in the rotary motor sector of *Escherichia coli* ATP synthase is 10. *PNAS* 98:4966–71
106. Mitome N, Suzuki T, Hayashi S, Yoshida M. 2004. Thermophilic ATP synthase has a decamer c-ring: indication of noninteger 10:3 H^+/ATP ratio and permissive elastic coupling. *PNAS* 101:12159–64
107. Stahlberg H, Müller DJ, Suda K, Fotiadis D, Engel A, et al. 2001. Bacterial Na^+-ATP synthase has an undecameric rotor. *EMBO Rep.* 2:229–33
108. Meier T, Morgner N, Matthies D, Pogoryelov D, Keis S, et al. 2007. A tridecameric c ring of the adenosine triphosphate (ATP) synthase from the thermoalkaliphilic *Bacillus* sp. strain TA2.A1 facilitates ATP synthesis at low electrochemical proton potential. *Mol. Microbiol.* 65:1181–92
109. Preiss L, Klyszejko AL, Hicks DB, Liu J, Fackelmayer OJ, et al. 2013. The c-ring stoichiometry of ATP synthase is adapted to cell physiological requirements of alkaliphilic *Bacillus pseudofirmus* OF4. *PNAS* 110:7874–79
110. Pogoryelov D, Yu J, Meier T, Vonck J, Dimroth P, Müller DJ. 2005. The c_{15} ring of the *Spirulina platensis* F-ATP synthase: F_1F_O symmetry mismatch is not obligatory. *EMBO Rep.* 6:1040–44
111. Pogoryelov D, Klyszejko AL, Krasnoselska GO, Heller EM, Leone V, et al. 2012. Engineering rotor ring stoichiometries in the ATP synthase. *PNAS* 109:e1599–608
112. Junge W, Pänke O, Cherepanov DA, Gumbiowski K, Müller M, Engelbrecht S. 2001. Inter-subunit rotation and elastic power transmission in F_OF_1-ATPase. *FEBS Lett.* 504:152–60
113. Hoppe J, Schairer HU, Friedl P, Sebald W. 1982. An Asp–Asn substitution in the proteolipid subunit of the ATP-synthase from *Escherichia coli* leads to a non-functional proton channel. *FEBS Lett.* 145:21–29
114. Lightowlers RN, Howitt SM, Hatch L, Gibson F, Cox GB. 1987. The proton pore in the *Escherichia coli* F_OF_1-ATPase: a requirement for arginine at position 210 of the α-subunit. *Biochim. Biophys. Acta* 894:399–406
115. Vik SB, Antonio BJ. 1994. A mechanism of proton translocation by F_1F_O-ATPase synthases suggested by double mutants of the α subunit. *J. Biol. Chem.* 269:30364–69
116. Meister M, Lowe G, Berg HC. 1987. The proton flux through the bacterial flagellar motor. *Cell* 49:643–50
117. Elston T, Wang H, Oster G. 1998. Energy transduction in ATP synthase. *Nature* 391:510–14
118. Miller MJ, Oldenburg M, Fillingame RH. 1990. The essential carboxyl group in subunit c of the F_1F_O-ATPase synthase can be moved and H^+-translocating function retained. *PNAS* 87:4900–4
119. Hatch LP, Cox GB, Howitt SM. 1995. The essential arginine residue at position 210 in the α subunit of the *Escherichia coli* ATP synthase can be transferred to position 252 with partial retention of activity. *J. Biol. Chem.* 270:29407–12
120. Langemeyer L, Engelbrecht S. 2007. Essential arginine in subunit a and aspartate in subunit c of F_OF_1 ATP synthase: effect of repositioning within helix 4 of subunit a and helix 2 of subunit c. *Biochim. Biophys. Acta* 1767:998–1005
121. Mitchell P. 1977. Epilogue: from energetic abstraction to biochemical mechanism. *Symp. Soc. Gen. Microbiol.* 27:383–423
122. DeLeon-Rangel J, Ishmukhametov RR, Jiang W, Fillingame RH, Vik SB. 2013. Interactions between subunits a and b in the rotary ATP synthase as determined by cross-linking. *FEBS Lett.* 587:892–97
123. Jiang WP, Fillingame RH. 1998. Interacting helical faces of subunits a and c in the F_1F_O ATP synthase of *Escherichia coli* defined by disulfide cross-linking. *PNAS* 95:6607–12
124. Fillingame RH, Steed PR. 2014. Half channels mediating H transport and the mechanism of gating in the F sector of *Escherichia coli* FF ATP synthase. *Biochim. Biophys. Acta* 1837:11305–10

125. Steed PR, Fillingame RH. 2014. Residues in the polar loop of subunit c in *Escherichia coli* ATP synthase function in gating proton transport to the cytoplasm. *J. Biol. Chem.* 289:2127–38
126. Gohlke H, Schlieper D, Groth G. 2012. Resolving the negative potential side (n-side) water-accessible proton pathway of F-type ATP synthase by molecular dynamics simulations. *J. Biol. Chem.* 287:36536–43
127. Emrich HM, Junge W, Witt HT. 1969. Artificial indicator for electric phenomena in biological membranes and interfaces. *Naturwissenschaften* 56:514–15
128. Schönknecht G, Junge W, Lill H, Engelbrecht S. 1986. Complete tracking of proton flow in thylakoids—the unit conductance of CF_O is greater than 10 fS. *FEBS Lett.* 203:289–94
129. Franklin MJ, Brusilow WS, Woodbury DJ. 2004. Determination of proton flux and conductance at pH 6.8 through single F_O sectors from *Escherichia coli*. *Biophys. J.* 87:3594–99
130. Feniouk BA, Kozlova MA, Knorre DA, Cherepanov D, Mulkidjanian A, Junge W. 2004. The proton driven rotor of ATP synthase: ohmic conductance (10 fS) and absence of voltage gating. *Biophys. J.* 86:4094–109
131. Xing J, Wang H, von Ballmoos C, Dimroth P, Oster G. 2004. Torque generation by the F_O motor of the sodium ATPase. *Biophys. J.* 87:2148–63
132. Deckers-Hebestreit G. 2013. Assembly of the *Escherichia coli* F_OF_1 ATP synthase involves distinct subcomplex formation. *Biochem. Soc. Trans.* 41:1288–93
133. Hilbers F, Eggers R, Pradela K, Friedrich K, Herkenhoff-Hesselmann B, et al. 2013. Subunit δ is the key player for assembly of the H^+-translocating unit of *Escherichia coli* F_OF_1 ATP synthase. *J. Biol. Chem.* 288:25880–94
134. Sambongi Y, Iko Y, Tanabe M, Omote H, Iwamoto-Kihara A, et al. 1999. Mechanical rotation of the c subunit oligomer in ATP synthase (F_OF_1): direct observation. *Science* 286:1722–24
135. Pänke O, Gumbiowski K, Junge W, Engelbrecht S. 2000. F-ATPase: specific observation of the rotating c subunit oligomer of EF_OEF_1. *FEBS Lett.* 472:34–38
136. Börsch M, Diez M, Zimmermann B, Reuter R, Gräber P. 2002. Stepwise rotation of the γ-subunit of EF_OEF_1-ATP synthase observed by intramolecular single-molecule fluorescence resonance energy transfer. *FEBS Lett.* 527:147–52
137. Diez M, Zimmermann B, Börsch M, Konig M, Schweinberger E, et al. 2004. Proton-powered subunit rotation in single-membrane-bound F_OF_1-ATP synthase. *Nat. Struct. Mol. Biol.* 11:135–41
138. Düser MG, Zarrabi N, Cipriano DJ, Ernst S, Glick GD, et al. 2009. 36 degrees step size of proton-driven c-ring rotation in FoF1-ATP synthase 2. *EMBO J.* 28:2689–96
139. Ishmukhametov R, Hornung T, Spetzler D, Frasch WD. 2010. Direct observation of stepped proteolipid ring rotation in *E. coli* F_OF_1-ATP synthase. *EMBO J.* 29:3911–23
140. Dimroth P, Wang H, Grabe M, Oster G. 1999. Energy transduction in the sodium F-ATPase of *Propionigenium modestum*. *PNAS* 96:4924–28
141. Aksimentiev A, Balabin IA, Fillingame RH, Schulten K. 2004. Insights into the molecular mechanism of rotation in the F_O sector of ATP synthase. *Biophys. J.* 86:1332–44
142. Pogoryelov D, Krah A, Langer JD, Yildiz O, Faraldo-Gómez JD, Meier T. 2010. Microscopic rotary mechanism of ion translocation in the F_O complex of ATP synthases. *Nat. Chem. Biol.* 6:891–99
143. Mukherjee S, Warshel A. 2012. Realistic simulations of the coupling between the protomotive force and the mechanical rotation of the F_O-ATPase. *PNAS* 109:14876–81
144. Petersen J, Forster K, Turina P, Gräber P. 2012. Comparison of the H^+/ATP ratios of the H^+-ATP synthases from yeast and from chloroplast. *PNAS* 109:11150–55
145. Laubinger W, Deckers-Hebestreit G, Altendorf K, Dimroth P. 1990. A hybrid adenosine triphosphatase composed of F_1 of *Escherichia coli* and F_O of *Propionigenium modestum* is a functional sodium ion pump. *Biochemistry* 29:5458–63
146. Cherepanov DA, Mulkidjanian A, Junge W. 1999. Transient accumulation of elastic energy in proton translocating ATP synthase. *FEBS Lett.* 449:1–6
147. Pänke O, Rumberg B. 1999. Kinetic modeling of rotary CF_OF_1-ATP synthase: storage of elastic energy during energy transduction. *Biochim. Biophys. Acta* 1412:118–28
148. Wächter A, Bi Y, Dunn SD, Cain BD, Sielaff H, et al. 2011. Two rotary motors in F-ATP synthase are elastically coupled by a flexible rotor and a stiff stator stalk. *PNAS* 108:3924–29

149. Saroussi S, Schushan M, Ben-Tal N, Junge W, Nelson N. 2012. Structure and flexibility of the c-ring in the electromotor of rotary F_OF_1-ATP of pea chloroplasts. *PLOS ONE* 7:e43045
150. Czub J, Grubmüller H. 2011. Torsional elasticity and energetics of F_1-ATPase. *PNAS* 108:7408–13
151. Rieger B, Junge W, Busch KB. 2014. Lateral pH gradient between OXPHOS complex IV and F_OF_1 ATP-synthase in folded mitochondrial membranes. *Nat. Commun.* 5:3103
152. Cherepanov DA, Junge W, Mulkidjanian AY. 2004. Proton transfer dynamics at the membrane/water interface: dependence on the fixed and mobile pH buffers, on the size and form of membrane particles, and on the interfacial potential barrier. *Biophys. J.* 86:665–80
153. Junge W. 1987. Complete tracking of transient proton flow through active chloroplast ATP synthase. *PNAS* 84:7084–88
154. Rumberg B, Becher U. 1984. Multiple ΔpH control of H^+-ATP synthase function in chloroplasts. In *H^+-ATPase (ATP Synthase): Structure, Function, Biogenesis. The F_OF_1 Complex of Coupling Membranes*, ed. S Papa, K Altendorf, L Ernster, L Packer, pp. 421–30. Bari, Italy: Adriat. Ed.
155. Junesch U, Gräber P. 1987. Influence of the redox state and the activation of the chloroplast ATP synthase on proton-transport-coupled ATP synthesis/hydrolysis. *Biochim. Biophys. Acta* 893:275–88
156. Mills JD, Mitchell P. 1982. Modulation of coupling factor ATPase activity in intact chloroplasts, reversal of thiol modulation in the dark. *Biochim. Biophys. Acta* 679:75–83
157. Werner-Grüne S, Gunkel D, Schumann J, Strotmann H. 1994. Insertion of a "chloroplast-like" regulatory segment responsible for thiol modulation into γ-subunit of F_OF_1-ATPase of the cyanobacterium *Synechocystis* 6803 by mutagenesis of *atpC*. *Mol. Gen. Genet.* 244:144–50
158. Bald D, Noji H, Stumpp MT, Yoshida M, Hisabori T. 2000. ATPase activity of a highly stable $\alpha_3\beta_3\gamma$ subcomplex of thermophilic F_1 can be regulated by the introduced regulatory region of γ subunit of chloroplast F_1. *J. Biol. Chem.* 275:12757–62
159. Bald D, Noji H, Yoshida M, Hirono-Hara Y, Hisabori T. 2001. Redox regulation of the rotation of F_1-ATP synthase. *J. Biol. Chem.* 276:39505–7
160. Konno H, Nakane T, Yoshida M, Ueoka-Nakanishi H, Hara S, Hisabori T. 2012. Thiol modulation of the chloroplast ATP synthase is dependent on the energization of thylakoid membranes. *Plant Cell Physiol.* 53:626–34
161. Khalili-Araghi F, Jogini V, Yarov-Yarovoy V, Tajkhorshid E, Roux B, Schulten K. 2010. Calculation of the gating charge for the Kv1.2 voltage-activated potassium channel. *Biophys. J.* 98:2189–98
162. Pullman ME, Monroy GC. 1963. A naturally occurring inhibitor of mitochondrial adenosine triphosphatase. *J. Biol. Chem.* 238:3762–69
163. Runswick MJ, Bason JV, Montgomery MG, Robinson GC, Fearnley IM, Walker JE. 2013. The affinity purification and characterization of ATP synthase complexes from mitochondria. *Open Biol.* 3:120160
164. Bason JV, Montgomery MG, Leslie AG, Walker JE. 2014. Pathway of binding of the intrinsically disordered mitochondrial inhibitorprotein to F1-ATPase. *PNAS* 111:11305–10
165. Nelson N. 1992. Evolution of organellar proton-ATPases. *Biochim. Biophys. Acta* 1100:109–24

RELATED RESOURCES

1. Original video recordings of the rotary motion of F_1: **http://www.k2.phys.waseda.ac.jp/Movies.html**
2. Original video recordings of F_OF_1: **http://www.home.uni-osnabrueck.de/wjunge/Media.html**
3. Animations of the rotary activity of F_1, F_O, and F_OF_1: **http://www.mrc-mbu.cam.ac.uk/research/atp-synthase/molecular-animations-atp-synthase**, **http://www.home.uni-osnabrueck.de/wjunge/Media.html**
4. Website dedicated to this enzyme: **http://www.atpsynthase.info**

Annual Review of Biochemistry
Volume 84, 2015

Contents

Indexes

Errata

An online log of corrections to *Annual Review of Biochemistry* articles may be found at http://www.annualreviews.org/errata/biochem